Interannual Variability of Upper-Troposphere Water Vapor Band Brightness Temperature

JOHN J. BATES

NOAA/ERL Climate Diagnostics Center, Boulder, Colorado

X. WU

Space Science and Engineering Center, University of Wisconsin-Madison, Madison, Wisconsin

D. L. JACKSON

Cooperative Institute for Research in the Environmental Sciences, University of Colorado, Boulder, Colorado

(Manuscript received 30 December 1994, in final form 7 August 1995)

ABSTRACT

A method for the intercalibration of the high-resolution infrared sounder (HIRS) upper-tropospheric water vapor band brightness temperature data is developed and applied to data from 1981 to 1993. Analysis of the adjusted anomaly time series show the location and strength of both the large-scale ascending and descending circulations in the Tropics as well as water vapor anomalies. Comparison of these HIRS data with outgoing longwave radiation and sea surface temperature anomalies reveals that both convection and increased upper-tropospheric moisture occur over anomalously warm water in the deep Tropics. The development and movement of deep convection and increased upper-tropospheric moisture can clearly be traced during the El Niño/Southern Oscillation warm events. These HIRS data are particularly useful in monitoring upper-tropospheric water vapor variability between the Tropics and subtropics.

1. Introduction

Water vapor is the predominant greenhouse gas and plays a major role in model simulations of future climate change due to man-made greenhouse gases. Observational studies (Stephens 1990) have found that a relationship exists between the precipitable water vapor and sea surface temperature (SST) such that a simple Clausius–Clapeyron relationship exists in the Tropics and subtropics. Global climate models also use such a relationship so that an initial SST increase due to man-made greenhouse gasses results in even more water vapor in the atmosphere in a positive feedback cycle. This water vapor feedback is responsible for a large (one-half to two-thirds) portion of the total global warming in many climate models. Although most of the precipitable water vapor is confined to the atmospheric boundary layer, the small amount of water vapor in the upper troposphere may contribute disproportionately (molecule for molecule) to the greenhouse effect.

Considerable controversy, however, exists about whether the upper-tropospheric water vapor content uniformly increases, as predicted in climate models (Cess et al. 1990) or whether the large-scale overturning circulations in the Tropics may actually lead to an overall drying in the upper troposphere (Lindzen 1990). The role of upper-tropospheric water vapor in climate has recently been explored using observational data (Wu et al. 1993; Soden and Bretherton 1993; Schmetz et al. 1994) in general circulation models (Soden and Bretherton 1994) and numerical weather prediction models (Hayden 1988; Eyre et al. 1993). Most of these studies, however, have used data for a relatively short period of time, often from only a single satellite. If long-term variability in upper-tropospheric water vapor is to be studied, such studies must use data from many instruments over time. Thus, the intercalibration of slightly different instruments and the absolute calibration of those instruments becomes critical for the analysis of interannual variability.

In this paper, we apply a method for the intercalibration of the upper-tropospheric water vapor band channel on the high-resolution infrared sounder (HIRS) instruments, hereafter called HIRS12. This method shares some of the methodology described below for ISCCP and MSU, but differs due to the unique

Corresponding author address: Dr. John J. Bates, NOAA/ERL/R/E/CD, 325 Broadway, Boulder, CO 80303-3328.
E-mail: bates@cdc.noaa.gov

characteristics of the HIRS water vapor band channels. These unique characteristics include an uncertainty in the absolute calibration of the HIRS water vapor band channels since the instruments were not calibrated in a vacuum chamber but rather in an open lab (i.e., an unknown amount of water vapor was present) and the lack of an in situ calibration standard since radiosonde measurements of upper-tropospheric water vapor are unreliable (Elliott and Gaffen 1992). Thus, this method provides a self consistent set of HIRS12 water vapor band observations suitable for studies of interannual variability, but lacks an absolute calibration to an in situ standard.

We argue that HIRS12 brightness temperature variability can be interpreted in the Tropics and subtropics in terms of both water vapor variability and dynamics. Wu et al. (1993) have demonstrated, using sensitivity studies, that variability of HIRS12 is largely due to water vapor profile variability and not to temperature profile variability. Thus, from approximately 30°N to 30°S, relatively high HIRS12 brightness temperatures indicate a relatively dry upper troposphere and relatively low HIRS12 brightness temperatures indicate a relatively moist upper troposphere.

The GOES and Meteosat geostationary satellite observations in sequential images of a water vapor channel nearly identical to HIRS12 have been used to track upper-tropospheric water vapor features and infer winds. Schmetz et al. (1994) have computed the mean monthly water vapor drift winds and divergence and compared this analysis with the monthly mean upper-tropospheric humidity derived from the water vapor band brightness temperatures. They found that the regions of divergence were highly correlated with maximum in upper-tropospheric moisture and regions of convergence were highly correlated with minimum in upper-tropospheric moisture. It is important to note that the divergence computed this way is on a constant water vapor mixing ratio surface, and not a constant pressure surface. Thus, we argue that the NOAA polar-orbiter HIRS12 data and anomalies can also be interpreted in terms of upper-tropospheric dynamics in the Tropics.

2. Dataset description

Several investigators have addressed the issue of intercalibration of different operational instruments on the NOAA series satellites. The NOAA series of satellites has operated since late 1978 with two sun-synchronous spacecraft; one in a morning/evening orbit and one in an afternoon/night orbit. The operational instruments include the Advanced Very High Resolution Radiometer (AVHRR) and the TIROS operational vertical sounder (TOVS). The TOVS is actually three instruments; the HIRS with 20 channels for sounding temperature and moisture profiles, the microwave sounding unit (MSU) with four broad temperature sounding channels, and the stratospheric sounding unit (SSU) a three-channel stratospheric temperature sounder. The International Satellite Cloud Climatology Project (ISCCP: Rossow and Schiffer 1991) has attempted to intercalibrate the visible channels on the AVHRR using a vicarious calibration since there is no onboard calibration target. This involves defining a baseline satellite, adjusting the other satellites to that baseline, and attempting in situ cross calibrations using aircraft underflights and stable, reflective ground targets. The TOVS instruments are calibrated continuously in orbit using cold space and onboard targets. Spencer and Christy (1992) describe a method for intercalibration of the different MSU instruments on the NOAA spacecraft over time using comparisons with in situ radiosonde temperature measurements. The HIRS instruments are calibrated separately from the MSU and examination of the onboard target indicates no long-term drift in any of the HIRS instruments used in this research.

The development of this dataset follows the methodology described in Wu et al. (1993; hereafter referred to as WBK93). We use the clear and cloud-cleared (up to 75% partial cloud cover) radiances from the National Environmental Satellite Data and Information Service (NESDIS) operational sounding product. WBK93 provide an extensive discussion of the errors involved in the production of the HIRS water vapor band brightness temperature climatology. The original dataset used by WBK93 was based on the period 1981–1988. This work adds the years 1989–1993 for a total of 13 years (eventually we hope to add the two earliest year of TOVS 1979 and 1980). Again, we apply extensive quality controls to the dataset and use adjustments as recommended in Appendix E of the NOAA Polar Orbiter Users Guide (Kidwell 1991).

Since we are using an operational product, there are data gaps caused not only by instrumental problems but also by problems within the operational processing data stream. We have found gaps ranging from several hours to slightly over a month in examining the operational sounding product record from 1981 to 1993. Raw HIRS radiance data (level 1b data) is available for many of these time periods, but as explained in WBK93, it is impractical for an individual researcher to process all this data. As part of the ECMWF reanalysis project, these gaps will be filled. Also, the TOVS Pathfinder project will be creating a new clear column radiance database for HIRS data in the future.

Conceptually, we view the variability in raw data as a combination of natural variability and bias. The bias may come from two sources. The "instrument bias" is due to the fact that the HIRS instrument (specifically, the spectral response function of the optical filter for HIRS Channel 12) onboard different satellites are not exactly the same. We first tried to remove this bias with a radiative transfer models. We used the model by Eyre (1991) with the spectral response function of the op-

tical filter for HIRS channel 12, and the TIROS initial guess atmospheres (TIGR: Monine et al. 1987). Mean HIRS12 brightness temperatures were computed for each of the seven NOAA spacecraft and each of the five TIGR airmasses. Differences in the computed brightness temperatures between the seven satellites were compared for each airmass, but the comparisons were inconclusive. We have also tried a much more accurate forward model (FASCODE3, Clough et al. 1988) on selected cases, but we still could not explain the differences between the satellites. A further examination of the HIRS prelaunch calibration, which produced the sensor response functions we used in the forward modeling, revealed that the calibration took place in an open laboratory (as opposed to a vacuum chamber) with the presence of an undetermined amount of water vapor (M. P. Weinreb, 1994, personal communication). This adds considerable uncertainty to the accuracy of the filter response function, and thus to determining relative instrument bias with radiative transfer model.

Since all of these datasets are derived from NOAA polar-orbiter satellite data, they may have correlated errors relative to in situ data as a result of instrument failure or orbital sampling times. The NOAA spacecraft are placed in a nominal sun-synchronous orbit, which means that the local time of sampling should not change over the life of the satellite. In fact, the equatorial crossing times of the different NOAA spacecraft drift in time and the original insertion times change slightly over the years. Figure 1 shows a plot of the drift of the ascending equatorial crossing times of the NOAA spacecraft. The time of initial insertion have changed for the afternoon/night spacecraft from 1430 LST for *NOAA-7,* 1420 for *NOAA-9,* and 1340 LST for *NOAA-11.* More disturbing, however, is the rate at which these spacecraft drift toward later local times. *NOAA-7* drifted later by 1 hr 30 min by the time *NOAA-9* became operational, and *NOAA-9* drifted later by nearly 2 h 30 min by the time *NOAA-11* became operational. However, *NOAA-11* has drifted the latest in time because of the launch failure of *NOAA-13. NOAA-11* has drifted from 1340 local time to about 1630 local time by January 1994 and is still drifting later. The morning satellites do not drift as fast. These drifts are present in all of the NOAA satellite products discussed here and so are correlated errors versus any in situ observations.

In addition to drifts, there are times when data from only a single satellite was available. This changes for each product. The SST data are only available since the launch of the *NOAA-7* spacecraft, the first spacecraft with a 5-channel AVHRR (see Bates 1994). The OLR dataset uses only data from the afternoon spacecraft except during parts of 1980 and 1981. During this time, the *TIROS-N* spacecraft failed (20 January 1980) and so the morning satellite (*NOAA-6*) was used until *NOAA-7* became available (19 August 1981).

Another source of bias, the "sampling bias," arises from the interaction between the satellite sampling characteristics and diurnal variability. Recall that the NOAA polar satellites are in sun-synchronous orbits that observe a fixed location on earth at fixed times (neglecting slow orbit drift). Recall also that the clear radiances used here are not available in areas of extensive cloud even if the clouds are confined in low levels.

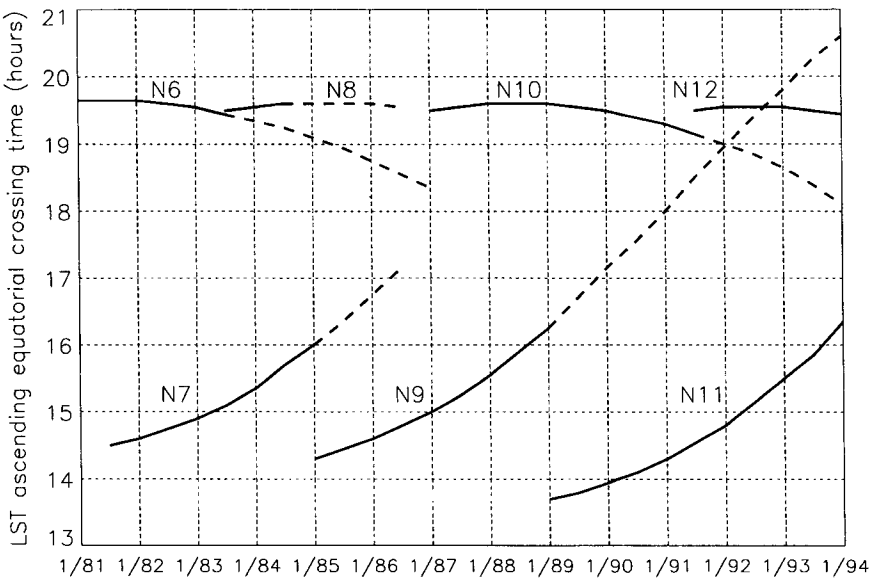

FIG. 1. Ascending node equatorial crossing times for the NOAA series satellites. The solid line indicates the period of operational coverage.

With these constraints, if for an area the cloud activity tends to obscure satellite observation at a certain time of the day during some season of the year, the satellite sampling will be implicitly biased. Another situation, in which the sampling is explicitly biased, is when there was only one satellite with HIRS instrument in operation, such as in 1985 and 1986.

Because of these characteristics of the bias in the time series of measurements from different satellites, we adjust the time series with an empirical method using two steps. First, the data were binned on 2.5 by 2.5 degree and 5-day average bins for each of the four possible passes per day. We then find the 13-yr mean for each location, for each pentad, and for each satellite pass. The anomaly relative to this mean is then computed for the 13-yr dataset. At this point we made an important assumption about the HIRS channel 12 brightness temperature, that is, if HIRS12 measurement by one of the satellite overpass at a certain location for a certain pentad is different from the relevant 13-yr mean, then the HIRS12 measurements by the other three satellite overpasses at the same location and for the same pentad should have the same amount of anomaly from their relevant 13-yr mean. In essence, we have assumed here that the interannual variation of the diurnal cycle is negligible.

Using this assumption, we claim that the anomaly we have obtained is to our best effort free of sampling bias. The second step is to distinguish the instrument bias from natural variability in the remaining anomaly. We did this empirically by comparing the anomalies by two satellites for the same target (same spatial coverage over the earth during same time period). We did not just compare the two means to derive relative bias; the assumption with that approach is that the measurements by two instruments differ by a fixed "offset." This may not be the case, as the instrument response to signal is highly nonlinear. Rather, we assume that the statistical distributions of anomalies by either instrument should be the same. Accordingly, we employed the "Empirical Distribution Function" (Weinreb et al. 1989) on the anomaly dataset.

Ideally, we would use one baseline satellite and adjust all other satellites to that baseline satellite. A practical difficulty is the lack of overlap period between satellites before *NOAA-8* and those after *NOAA-9*. This is primarily due to the premature loss of *NOAA-8* before the launch of *NOAA-9*. During that period, *NOAA-6* was reactivated, but the HIRS instrument was too noisy and could not be used. As a result, we were forced to construct two time series, one based on *NOAA-7* and the other based on *NOAA-10*. We then inspected time-latitude diagrams and joined the two time series by an ad hoc adjustment of 0.4°C to the latter time series. Finally, the four adjusted anomalies were averaged to yield a single anomaly for each location and for each pentad, which should contain only the natural variability.

Figure 2 shows the cumulative empirical distribution function (EDF) for the overlap periods between the different spacecraft used in this study; one line for each local overpass time for each satellite. The overlap time between *TIROS-N* and *NOAA-6* was for the first six weeks of 1981, and so we attribute the scatter between those instruments to an insufficient number of samples to completely populate the EDF. Our work suggests that greater than 500 000 samples are needed to form a stable EDF. The EDFs between *NOAA-6* and *NOAA-7, NOAA-7* and *NOAA-8,* and *NOAA-10* and *NOAA-11* all are very stable and show there are only small intersatellite calibration differences between these instruments. The largest differences are found between *NOAA-9* and *NOAA-10.* Since the *NOAA-10* and *NOAA-11* plot shows very good agreement between that pair of instruments, we conclude that the calibration of the HIRS-12 channel on *NOAA-9* was highly anomalous. Figure 3 shows the cumulative EDFs for each local orbit time for each pair of overlapping instruments. The instruments generally show good agreement indicating stable intersatellite calibrations throughout the entire time period. The exceptions again are *TIROS-N* and *NOAA-9,* as discussed above.

One other intersatellite calibration issue is possible—long-term drift between instruments during the overlap periods. This was examined in a manner similar to Spencer and Christy (1992). Figure 4 shows a plot of the HIRS12 signal-to-noise ratios {S/N = [variance(intersatellite anomaly sums)]/[variance (intersatellite anomaly differences)]} for the 28-month overlap period between *NOAA-11* and *NOAA-12*. There is a large variability in the structure of the S/N that provides important information on the utility of these data. The signal, the HIRS12 radiances, are influenced by both the moisture and temperature profile. Within the Tropics, the response of HIRS12 to moisture variations is quite large (see WBK93 for details), but in the extratropics it is relatively small. The noise level of HIRS12 depends on both the instrument noise and cloud-clearing algorithm and is estimated by WBK93 to be 2.48 K for single observations within a grid box and 1.11 K for five observations within a grid box. Thus, in the extratropics the HIRS12 S/N is low; ranging between 1 and 5. Within the Tropics (30°N–30°S), the signal is higher and S/N values are generally greater than 5. The spatial pattern within the Tropics is dominated by the variability of the noise, which is directly related to the number of observations. In general, there are fewer observations in the regions of persistent monsoon cloudiness than in the clear regions.

The results of this adjustment process are summarized in Table 1 for the region 30°N to 30°S. In general, the adjustment is at most about 0.25°C. The only exception is the *NOAA-9* adjustment, which is between 0.40° and 0.45°C. As described above we believe that the *NOAA-9* calibration was highly anomalous. To apply the EDF adjustment, a lookup table is formed be-

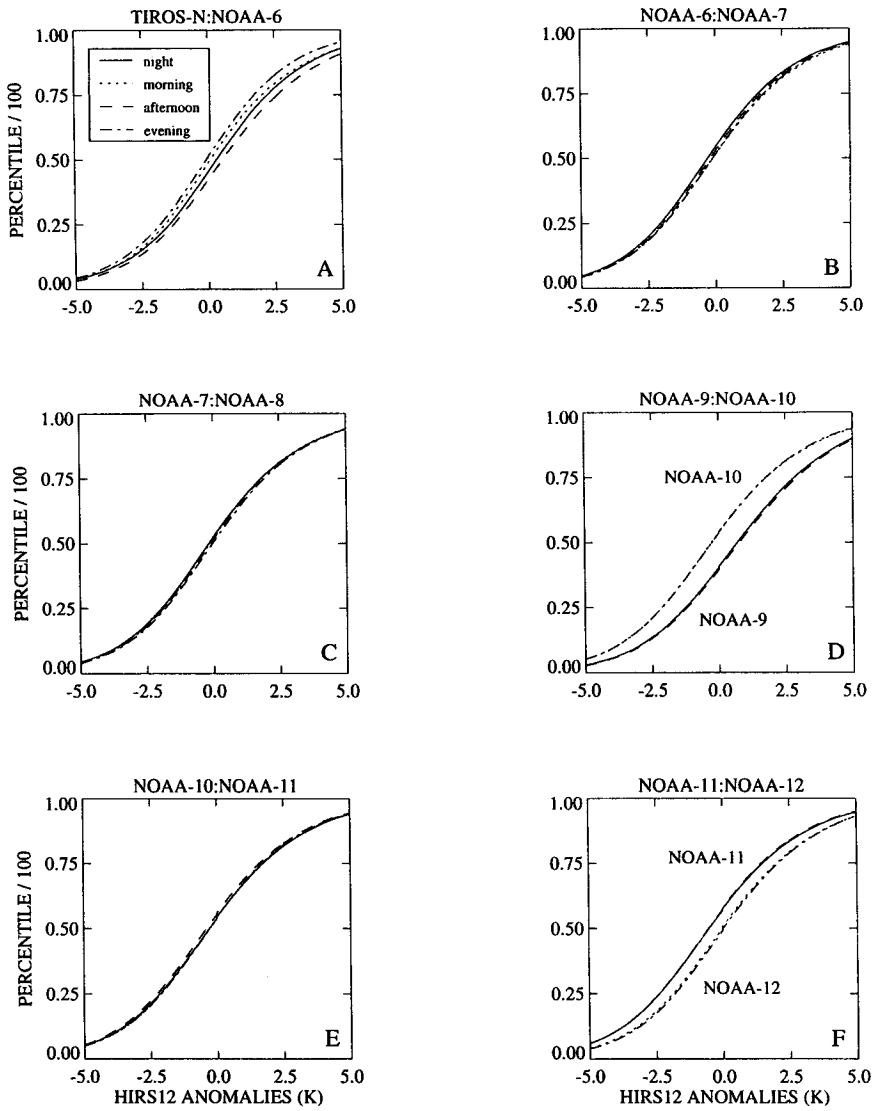

FIG. 2. Cumulative EDF for overlap periods between different instruments including (a) *TIROS-N:NOAA-6,* (b) *NOAA-6:NOAA-7,* (c) *NOAA-7:NOAA-8,* (d) *NOAA-9:NOAA-10,* (e) *NOAA-10:NOAA-11,* and (f) *NOAA-11:NOAA-12.*

tween the reference satellite and pass and the other three passes. An example of one of the lookup tables generated by this process is shown in Fig. 5. It shows the EDF adjustment for the *NOAA-10/NOAA-11* overlap period. For this time period, the adjustment is basically a small linear offset for the two instruments.

3. Relationship to other tropical climate indices

To assess the information content of the upper-tropospheric water vapor band brightness temperature climatology (HIRS12), in this section we compare it to the blended sea surface temperature anomalies (SSTs; Reynolds and Smith 1994), and outgoing longwave radiation anomalies (OLRs; Gruber and Winston 1978). All of these indices use data from the NOAA polar-orbiting spacecraft. The SST and OLR datasets use data from the Advanced Very High Resolution Radiometer (AVHRR) on the primary NOAA spacecraft. The primary NOAA spacecraft is defined as the afternoon satellite (i.e., *TIROS-N, NOAA-7, NOAA-9, NOAA-11*), unless the afternoon satellite is not available, in which case it becomes the morning satellite. Chellia and Arkin (1992) have shown that changes in the OLR sampling time can be identified in the analysis of the time series an empirical orthogonal function (EOF) decomposition of the dataset. We have removed this anomaly in the OLR time series by reconstructing the time series

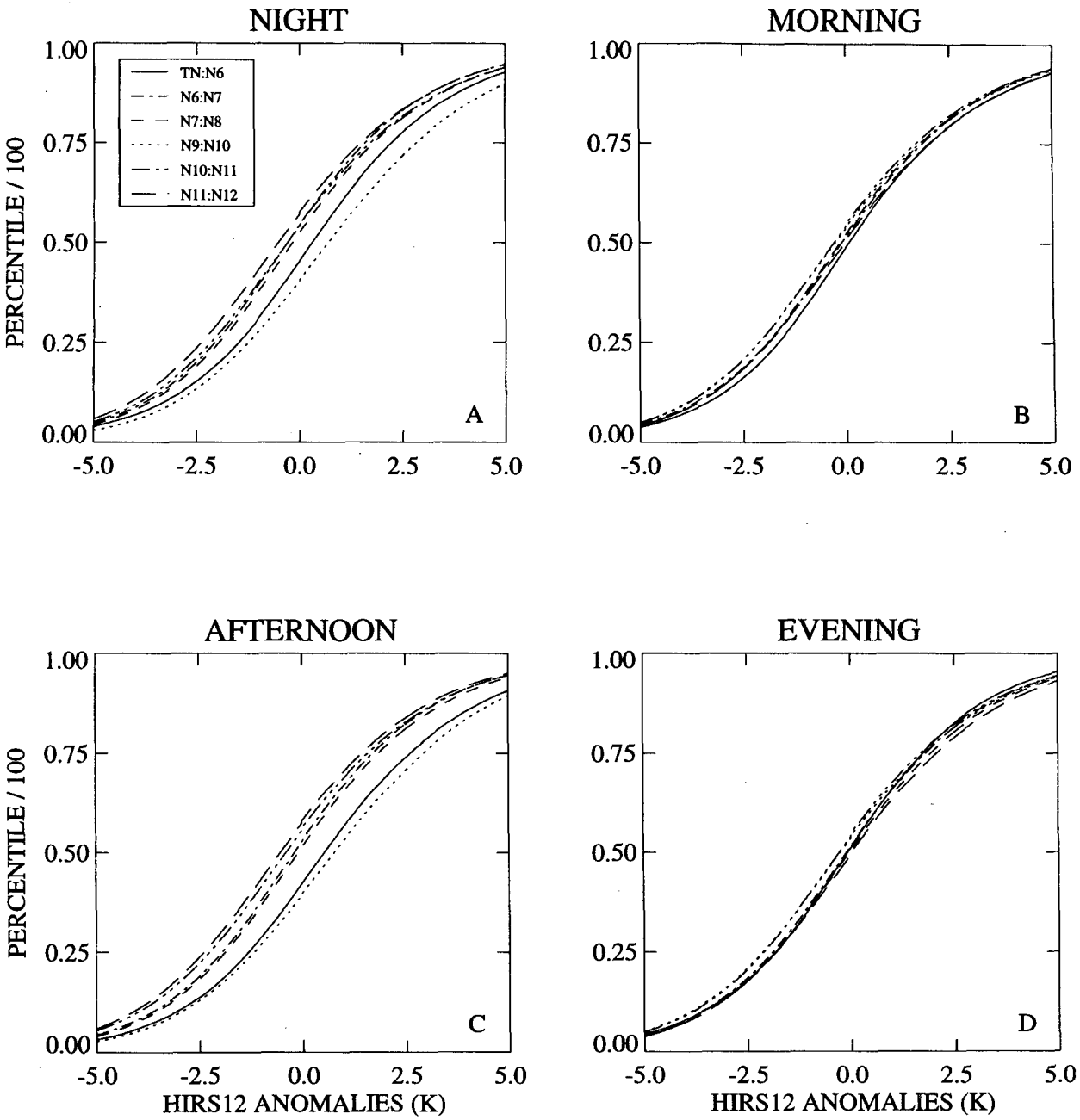

FIG. 3. Cumulative EDF for all overlap periods as a function of equatorial crossing time.

without this EOF mode. The SST blending scheme of Reynolds and Smith (1994) effectively removes biases (such as those caused by volcanic aerosol events) in the satellite-only SST retrieval by tuning to in situ SST observations.

a. Analysis of time/longitude variability

Figure 6 shows monthly mean anomaly time/longitude sections of SST, OLR, and HIRS12 averaged from 10°N to 10°S. All fields show large interannual variability related to El Niño/Southern Oscillation (ENSO) warm and cold events. ENSO warm events occurred in 1982/83, 1987, and 1991/92; and cold events occurred in 1984/85 and 1988/89. OLR variability is dominated by anomalous presence or lack of high cloudiness associated with deep convection. In regions with little deep convection, such as the subtropics, there is little OLR variability. Thus, the OLR anomalies are associated with shifts in deep convection

from over the western Pacific-eastern Indian Ocean warm pool to the central and eastern Pacific Ocean. For example, during 1983 large negative anomalies of OLR are found over the central and eastern Pacific Ocean and large positive anomalies are found in the western Pacific. Note that the large OLR anomalies are confined between 90°E and 90°W longitudes because variability of deep convection is greatest there.

The time-longitude section of HIRS12 anomalies shows a pattern evolution similar to OLR, but shows equal intensities in anomalies regardless of longitude. This is because HIRS12 is a sounding channel that always peaks in the upper troposphere and so is much more closely associated with circulation features than OLR. Negative HIRS12 anomalies are associated with greater upper-tropospheric moisture and, in studies using upper-tropospheric water vapor as a passive tracer of winds (Schmetz et al. 1994), anomalous divergence. Similarly, positive HIRS12 anomalies are associated with lower values of upper-tropospheric moisture and anomalous convergence. With this in mind, comparisons between the OLR and HIRS12 time-longitude sections reveal important differences in the evolution of the ENSO warm and cold events over the past 13 years.

During the 1982/83 warm event, the HIRS12 data shows three distinct shifts in the high and low moisture maximum. In early 1982, there is enhanced moisture at 135°E and decreased moisture between 135° and 90°W. In late 1982, negative OLR anomalies (indicating anomalous high clouds) and negative HIRS12 brightness temperature anomalies (indicating anomalously high moisture and divergence) are found between 180° and 135°W, and positive anomalies are centered between 135°E and 180°, indicating a major shift in the location of deep convection. In mid-1983, the HIRS12 data show a distinct move of the center of anomalous high moisture to 90°W and a center of anomalous low moisture of nearly the same intensity centered at 45°W. In contrast, the OLR data show much weaker anomalies in these regions because of a lack of high cloud variability.

During the evolution of the 1986/87 warm event, the OLR and HIRS12 anomalies again show similar patterns of evolution with negative OLR and HIRS12 anomalies beginning in 1984 at 120°E until late 1986 when the anomalies move east to the dateline. Larger differences in the OLR and HIRS12 anomaly pattern evolution are found during 1989–1991 leading up to

TABLE 1. Intersatellite adjustments for the HIRS12 channel on the NOAA spacecraft from 1981 to 1994 from 30°N to 30°S.

Mean monthly difference (°C)	Satellite	Year	Pentad (start–finish)	Reference satellite
0.15	TN to N6	81	1–45	N6 to N7
0.25	N6 to N7	81	46–73	N7
		82	1–73	
		83	1–34	
0.10	N8 to N7	83	35–73	N7
		84	1–34	
0.40	N9	84	35–73	ad hoc
		85	1–73	
		86	1–73	
		87	1–3	
0.45	N9 to N10	87	4–73	N10
		88	1–3	
−0.03	N11 to N10	88	4–73	N10
		89	1–73	
		90	1–73	
		91	1–4	
0.26	N12 to N11	91	5–73	N11 to N10
		92	1–73	
		93	1–73	

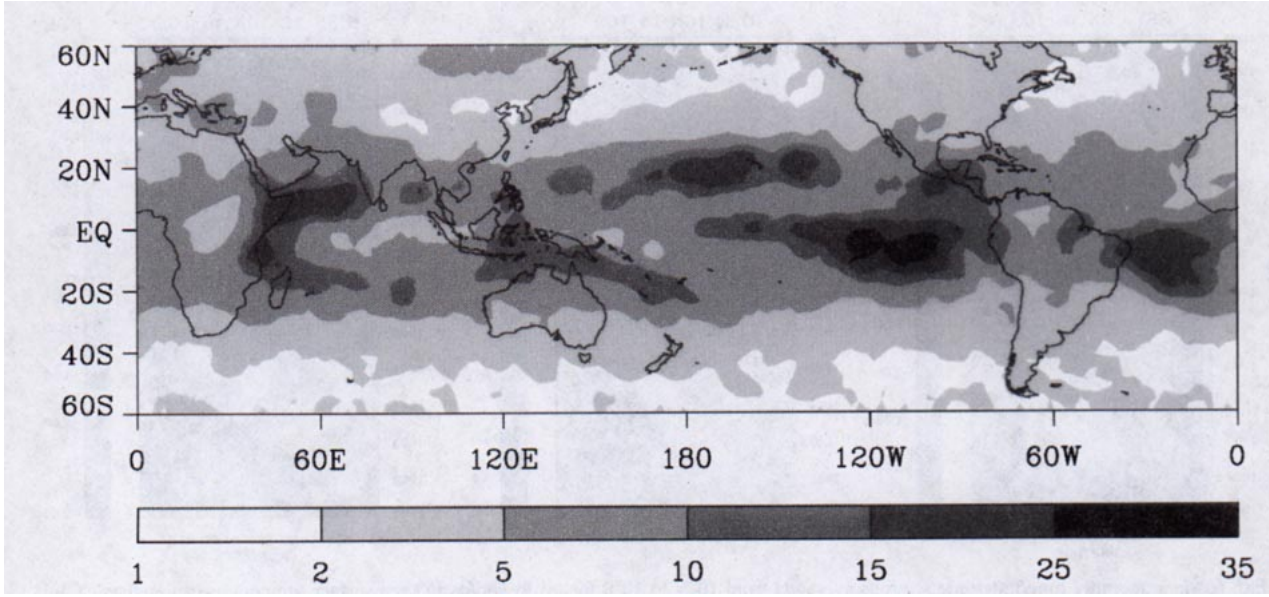

FIG. 4. Signal-to-noise ratio of HIRS12 gridpoint anomaly differences between *NOAA-11:NOAA-12* for a 28-month overlap period.

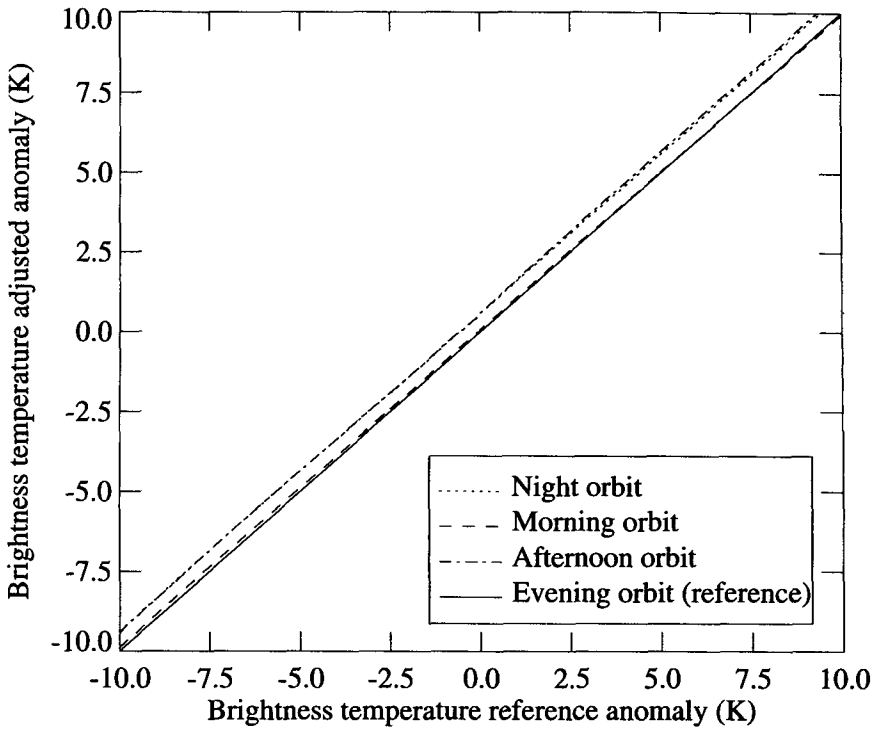

FIG. 5. Anomaly adjustment look-up table for *NOAA-10:NOAA-11* overlap based on the EDF.

the 1991/92 warm event. The OLR data show a large positive anomaly at 180° throughout 1989, but the HIRS12 data show only a weak anomaly. In 1991, the HIRS12 data show a large positive anomaly between 180° and 90°W where the OLR data show only weak anomalies. It is not clear why there are relatively larger differences between these two datasets at these times. During 1992 and 1993 the OLR and HIRS12 anomaly patterns again are quite similar. Both show anomalous deep convection and high moisture in the eastern Pacific and anomalous suppression of convection and low moisture in the western Pacific.

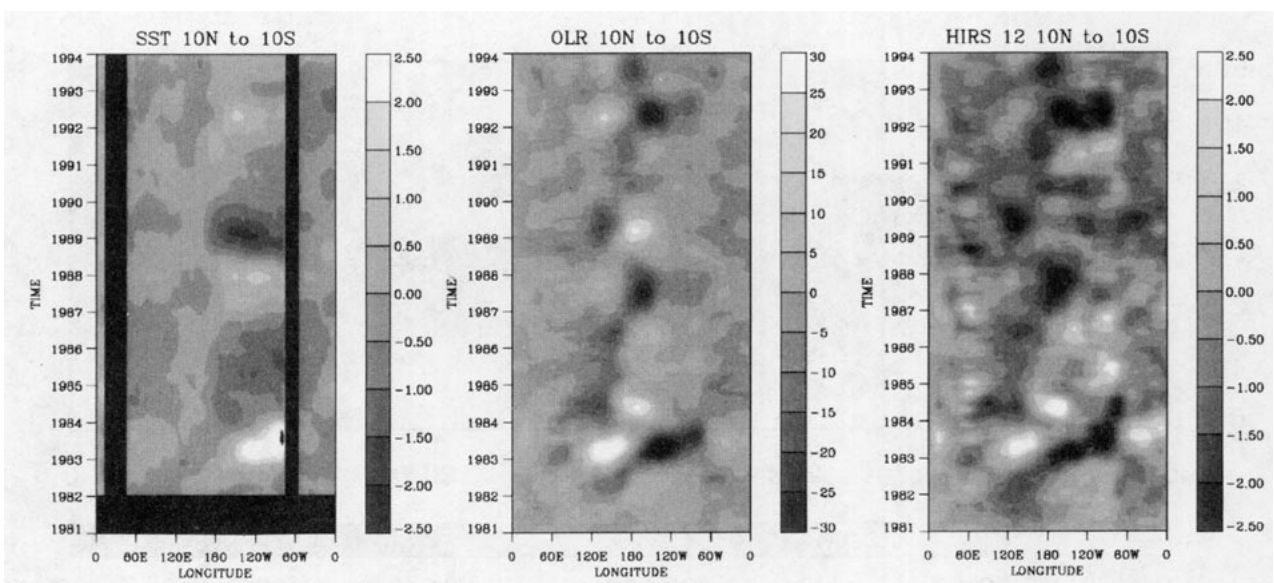

FIG. 6. Mean monthly time/longitude sections averaged from 10°N to 10°S for (a) Reynolds I/O sea surface temperature anomalies (°C), (b) outgoing longwave radiation anomalies (W m^{-2}), and (c) HIRS12 water vapor brightness temperature anomalies (°C).

Figure 7 shows HIRS12 anomaly time-longitude sections for three latitude strips; 30°–10°N (Fig. 7a), 10°N–10°S (Fig. 7b), and 10°–30°S (Fig. 7c). In the northern subtropics (Fig. 7a) the majority of the variability is centered at 135°W and extends from about 180° to 90°W. Variability near 135°W at these latitudes is generally out of phase with variability at 135°W in the deep Tropics (Fig. 7b). Thus, during the strong 1982/83 warm event, HIRS12 is anomalously low (moist) in the Tropics, but anomalously high (dry) in the northern subtropics. In the southern subtropics (Fig. 7c), the major variability is found between 90°E and 90°W. Again, this variability is generally out of phase with variability in the Tropics (Fig. 7b) but shows propagation of anomalies during ENSO events. This is in contrast to the northern extratopics, which shows standing variability near 135°W.

b. *Empirical orthogonal function analysis*

Empirical orthogonal function (EOF) analysis was performed separately on each of the monthly mean anomaly datasets. To keep the comparisons uniform, the data were analyzed from 1982 to 1993 (since the satellite SST data only begin in 1982) for the tropical region 30°N–30°S. In all cases, the first mode is associated with interannual, global variability during ENSO warm events. Because of this, the principal component time series for each dataset has been plotted on a single figure (Fig. 8d). It should be noted, however, that the principal component time series for each field is associated only with the eigenvector map for that field (i.e., the SST anomaly principal component time series, the dashed line in Fig. 8d, only applies to the SST anomaly eigenvector field of Fig. 8a). The amount of variance explained by the first mode ranges from 12% for the HIRS12, to 24% for the OLR, and to 32% for the SST. Contemporaneous cross correlations between the amplitudes of the leading modes are shown in Table 2. All the correlations are significant at the 99% level assuming only 72 degrees of freedom (half the total number of months). Correlations are quite high between OLR, HIRS12, and the SST anomalies (.86 and .78), but the highest correlations are found between the OLR and HIRS12 (.93).

The spatial patterns of the leading mode for each parameter are shown in Figs. 8a–c. The classic ENSO warm event SST signature (Fig. 8a) is evident with positive anomalies in the central and eastern equatorial Pacific and negative anomalies in the western equatorial Pacific extending poleward to the extratropics. This interannual SST EOF pattern has been found in independent analysis of ship-only data and satellite-only data (Bates 1994). The spatial pattern for OLR anomalies (Fig. 8b) shows a pattern of near-equatorial anomalies that results from the shift of convection from the western Pacific Ocean to the central and eastern Pacific during warm events. There are positive OLR anomalies centered near the dateline and extending into the eastern equatorial Pacific. Negative OLR anomalies are found in the western equatorial Pacific, and there is a small negative anomaly over northeastern Brazil.

The spatial pattern of the HIRS12 EOF (Fig. 8c) shows some similar features, but also some distinctly different features when compared to the OLR. Along the equator in the Pacific Ocean, the HIRS12 and OLR features are most similar. At the equator and the dateline, there is a minimum in HIRS12. The minimum extends eastward to a second minimum in the eastern Pacific. Relative maximum along the equator are found

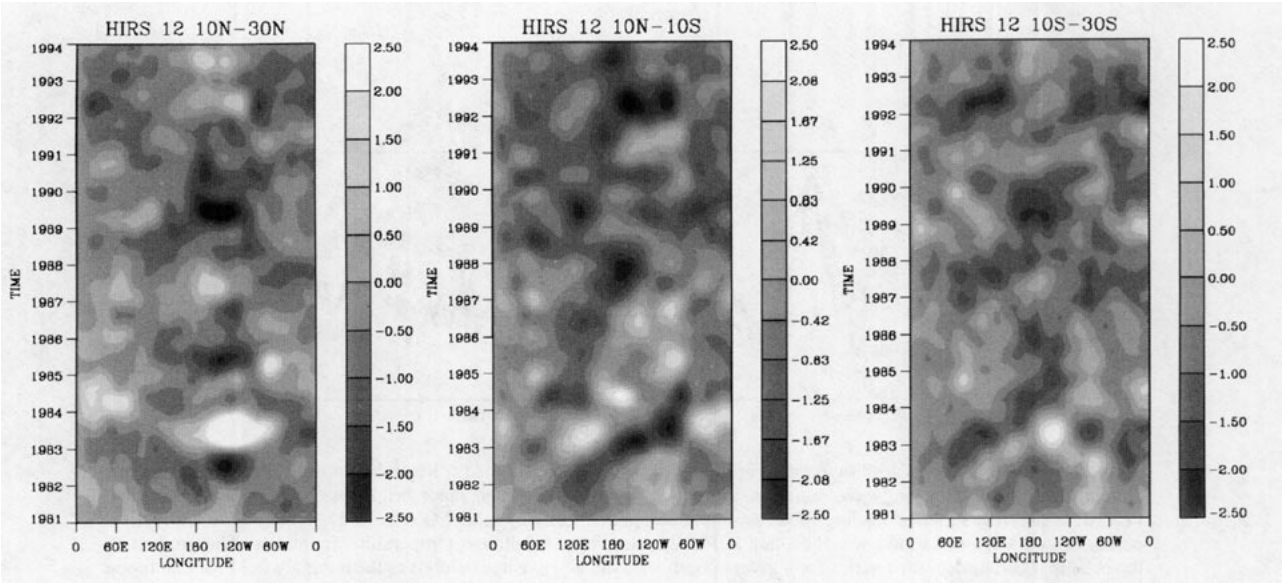

FIG. 7. Mean monthly time/longitude sections for HIRS12 (°C) for (a) 30°–10°N, (b) 10°N–10°S, and (c) 10°–30°S.

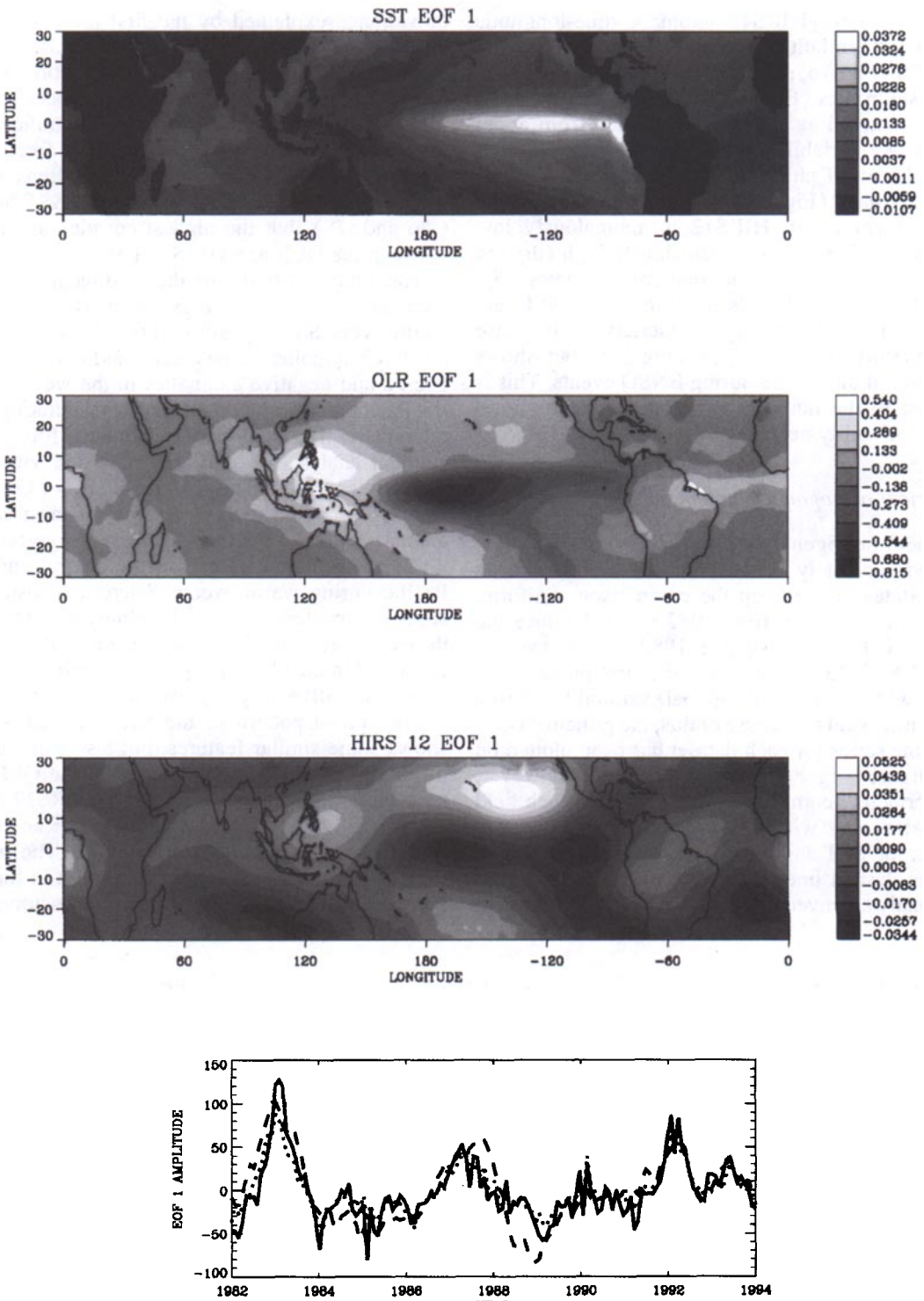

FIG. 8. Spatial pattern of leading mode empirical orthogonal function for (a) Reynolds I/O sea surface temperature anomalies, (b) outgoing longwave radiation anomalies, (c) HIRS12 water vapor brightness temperature anomalies. Plot (d) is the time series of leading mode principal component for Reynolds I/O sea surface temperature anomalies, outgoing longwave radiation anomalies, and HIRS12 water vapor brightness temperature anomalies. The product of the principal component time series for a given month with the eigenvector field gives the anomaly field for that mode and month. The units for this product are °C for the Reynolds I/O sea surface temperature anomalies, W m^{-2} for the outgoing longwave radiation anomalies, and °C for the HIRS12 water vapor brightness temperature anomalies.

TABLE 2. Contemporaneous cross correlation between the leading mode empirical orthogonal function time series 1982–1994.

	HIRS12	SST	OLR
HIRS12		−0.78	−0.93
SST			0.86

in the western Pacific and across South America extending over northeast Brazil. The most striking difference between the HIRS12 and OLR, however, occurs in the subtropical latitudes. A large maximum in HIRS12 is found just southeast of Hawaii. There is only a weak hint of this anomaly in the OLR data. The HIRS12 data also show a series of maximum and minimum across the Southern Hemisphere subtropics including a minimum from southwestern Australia extending westward toward Madagascar, a maximum to the east of Australia, and two minima farther east, one on either side of South America.

4. Discussion

OLR anomalies have been used extensively as a surrogate for anomalous presence or absence of deep convection in the Tropics. In these applications, OLR is an active tracer of high, cold clouds and as a result there is little OLR variability where there is little high cloud variability. In contrast, HIRS12 is a passive tracer of upper-tropospheric water vapor. However, interpretation of HIRS12 anomalies is complex and depends on both the temperature and moisture profile. The noise level of HIRS12 is relatively high and results from both instrument noise and noise due to cloud clearing. The HIRS12 signal is relatively low in the extratropics leading to relatively low signal-to-noise ratios. Within the Tropics, the HIRS12 signal is relatively larger and, since it is a passive tracer, its variability is more equally distributed throughout the Tropics. This makes HIRS12 anomalies a much better surrogate for tracing circulation anomalies in the Tropics than OLR anomalies. Even in the Tropics, however, the HIRS12 anomalies have a complex signal-to-noise ratio structure due to cloudiness. This complex structure should be used when assimilating HIRS12 data into numerical models and in schemes that merge different sources of water vapor information to provide global merged products.

As more long-term datasets from satellite remote sensing become available, analysis of these datasets must focus not only on interannual processes that can be observed, but also on how applicable the physics of the retrieval process is for studying such processes. From the discussion above, it is clear that the HIRS12 dataset provides unique, as well as complimentary, information about the tropical upper-tropospheric water vapor content and dynamics. It is most similar to the OLR data in the equatorial Pacific sector, but provides unique information about the strength of the dry, descending branches of the large-scale overturning cells in the Tropics.

5. Conclusions

Analysis of HIRS12 data reveals that it has high precision but a rather uncertain overall calibration. This causes a problem when attempting to study interannual variability since it makes the intercalibration of many instruments impossible from first principle radiative transfer physics. In addition, there is no reliable in situ upper-tropospheric water vapor data to use as a transfer standard for the different satellite instruments. As a result, we have developed and applied an ad hoc technique to adjust the different satellites to a set of baseline satellites. The adjusted time series of HIRS12 observations appears acceptable for studies of interannual variability in the Tropics and subtropics.

To first order, HIRS12 brightness temperature anomalies in the Tropics and subtropics can be interpreted in terms of both upper-tropospheric water vapor and circulation anomalies. This is because sensitivity studies using realistic tropical temperature and water vapor profiles demonstrate that HIRS12 brightness temperature variations are quite sensitive to water vapor variations but rather insensitive to temperature variations. On the GOES and Meteosat geostationary spacecraft, data from channels similar to HIRS12 have been used to track upper-tropospheric water vapor features. Comparison of monthly mean upper-tropospheric water vapor drift winds and the retrieved upper-tropospheric humidity revealed that the moisture maximum are associated with divergent flow and moisture minimum are associated with convergent flow. We thus argue that HIRS12 brightness temperature anomalies can be interpreted in a similar way and thus be used to diagnose upper-tropospheric dynamic anomalies. Since the HIRS12 weighting function peaks at lower pressures in moist upper-tropospheric conditions (about 200–300 mb) and at higher pressures in dry upper-tropospheric conditions (about 300–400 mb), these dynamic anomalies are with respect to a constant water vapor mixing ratio surface and not along constant pressure surfaces.

The comparison of HIRS12, OLR, and SST anomaly data shows that both convection and increased moisture occur over anomalously warm water in the deep Tropics from 10°N to 10°S. The movement of the deep convection and increased upper-tropospheric moisture can be clearly traced during the ENSO warm events of 1982/83, 1986/87, and 1991/93. The HIRS12 data also clearly depict the intensity and locations of the dry, subsiding branches of the tropical circulations. During the evolution of the 1982/83 warm event, the anomalous drying shifts from west of the convection early in the event to east of the convection late in the event.

HIRS12 anomalies are particularly useful in monitoring upper-tropospheric water vapor changes be-

tween the Tropics and subtropics. Time-longitude sections of HIRS12 anomalies in the deep Tropics (10°N–10°S) versus the subtropics (30°–10°N and 10°–30°S) reveal that anomalies in the subtropics are generally out of phase with anomalies in the deep Tropics. However, there is considerable difference in the behavior of the Northern Hemisphere subtropics versus the Southern Hemisphere subtropics. In the Southern Hemisphere subtropics, there is a clear propagation of anomalies out of phase with the deep Tropics. In the Northern Hemisphere subtropics, there is only a standing anomaly pattern centered at 135°W.

Empirical orthogonal function analysis of these datasets reveals global teleconnection patterns in the upper troposphere in the Tropics and subtropics during ENSO warm events. Increased upper-tropospheric moisture accompanies the increased convection in the central and eastern equatorial Pacific and decreased moisture is found over the western equatorial Pacific. More importantly, the subtropic and global tropic anomalies are as intense as those in the equatorial Pacific basin. These anomalies include very strong drying through the northeastern Pacific Ocean and weaker drying in the southwestern Pacific Ocean and over northeast Brazil extending east into southern Africa. Anomalous high water vapor is found extending northeast and southeast from the eastern tropical Pacific into the North and South Atlantic and from southwestern Australia northwest into the south Indian Ocean. Thus, HIRS12 data have the potential to help us better understand teleconnections from the areas of anomalous convection to distant locations in the Tropics and subtropics.

For the future, we are working on methods to separate the water vapor signal from the temperature signal in HIRS12 so that we can produce a climatology of upper-tropospheric water vapor and examine its relation to the earth's radiation budget. In addition, this work shows that we clearly need improved observations of upper-tropospheric water vapor from in situ sensors. This is required to improve the absolute calibration of the HIRS12 data and to be used as a standard for intercalibration of the different HIRS12 instruments. There are also many more studies that can be performed just using the HIRS12 brightness temperature data. These include studies of whether the HIRS12 data can be used to better predict global teleconnection pattern evolution during ENSO warm events and to study high-frequency variability.

Acknowledgments. This work would not have been possible without the computer programming efforts of Cathy Cormack and Wendy Sullivan. Portions of this dataset were supplied by S. J. S. Khalsa, G. Stephens, and I. Wittmeyer. Information on the drift of the NOAA polar-orbiting spacecraft was provided by NOAA/NESDIS spacecraft operations center.

REFERENCES

Bates, J. J., 1994: A decade of sea surface temperature observations from space. *Adv. Space Res.*, **14,** (3)5–(3)14.

Cess, R. D., and Coauthors, 1990: Intercomparison and interpretation of climate feedback processes in 19 atmospheric general circulation models. *J. Geophys. Res.*, **95,** 16 601–16 615.

Chelliah, M., and P. A. Arkin, 1992: Large-scale interannual variability of monthly outgoing longwave radiation anomalies over the global Tropics. *J. Climate,* **5,** 371–389.

Clough, S. A., F. X. Kneizys, G. P. Anderson, E. P. Shettle, J. H. Chetwynd, L. W. Abreu, L. A. Hall, and R. D. Worsham, 1988: FASCODE3: Spectral simulation. *IRS '88: Current Problems in Atmospheric Radiation,* J. Lenoble and J.-F. Geleyn, Eds., Lille, France.

Elliott, W. P., and D. J. Gaffen, 1991: On the utility of radiosonde humidity archives for climate studies. *Bull. Amer. Meteor. Soc.,* **72,** 1507–1520.

Eyre, J. R., 1991: A fast radiative transfer model for satellite sounding systems. ECMWF Tech. Memo. 176, 26 pp.

——, G. A. Kelly, A. P. McNally, E. Andersson, and A. Persson, 1993: Assimilation of TOVS radiance information through one-dimensional variational analysis. *Quart. J. Roy. Meteor. Soc.,* **119,** 1427–1463.

Gruber, A., and J. S. Winston, 1978: Earth–atmosphere radiative heating based on NOAA scanning radiometer measurements. *Bull. Amer. Meteor. Soc.,* **59,** 1570–1573.

Hayden, C. M., 1988: GOES-VAS simultaneous temperature-moisture retrieval algorithm. *J. Appl. Meteor.,* **27,** 705–733.

Kidwell, K. B., 1991: *NOAA Polar Orbiter Users' Guide.* NOAA/National Environmental Satellite, Data, and Information Service, 204 pp.

Lindzen, R. S., 1990: Some coolness concerning global warming. *Bull. Amer. Meteor. Soc.,* **71,** 288–299.

Monine, P., A. Chedin, and N. A. Scott, 1987: Automatic classification of air mass type from satellite vertical sounding data: Application to *NOAA-7* observations. *Ocean–Air Interactions,* **1,** 95–108.

Reynolds, R. W., and T. M. Smith, 1994: Improved global sea surface temperature analysis using optimal interpolation. *J. Climate,* **7,** 929–937.

Rossow, W. B., and R. A. Schiffer, 1991: ISCCP cloud data products. *Bull. Amer. Meteor. Soc.,* **72,** 2–18.

Schemtz, J. C. Geijo, K. Holmlund, and L. Van de Berg, 1994: Wind fields and upper tropospheric humidity from the METEOSAT water vapor channel. *Seventh Conf. on Satellite Meteorology and Oceanography,* Monterey, CA, Amer. Meteor. Soc., 96–97.

Soden, B. J., and F. P. Bretherton, 1993: Upper tropospheric relative humidity from the GOES 6.7 μm channel: Method and climatology for July 1987. *J. Geophys. Res.,* **98,** 16 669–16 688.

——, and ——, 1994: Evaluation of the water vapor distribution in general circulation models using satellite observations. *J. Geophys. Res.,* **99,** 1187–1210.

Spencer, R. W., and J. R. Christy, 1992: Precision and radiosonde validation of satellite gridpoint temperature anomalies. Part I: MSU channel 2. *J. Climate,* **5,** 847–857.

Stephens, G. L., 1990: On the relationship between water vapor over the oceans and sea surface temperature. *J. Climate,* **3,** 634–645.

Weinreb, M. P., R. Xie, J. H. Lienesh, and D. S. Crosby, 1989: Destriping GOES images by matching empirical distribution functions. *Remote Sens. Environ.,* **29,** 185–195.

Wu, X., J. J. Bates, and S. J. S. Khalsa, 1993: A climatology of the water vapor band brightness temperatures from NOAA operational satellites. *J. Climate,* **6,** 1282–1300.